Journal of Tissue Engineering
Volume 7: 1–8
Reprints and permissions:
sagepub.co.uk/journalsPermissions.nav

DOI: 10.1177/2041731415626018
tej.sagepub.com
SAGE

Porcine acellular lung matrix for wound healing and abdominal wall reconstruction: A pilot study

Joseph S Fernandez-Moure[1,2], Jeffrey L Van Eps[1,2], Jessica R Rhudy[3], Fernando J Cabrera[2], Ghanashyam S Acharya[4], Ennio Tasciotti[2], Jason Sakamoto[3] and Joan E Nichols[5]

Abstract

Surgical wound healing applications require bioprosthetics that promote cellular infiltration and vessel formation, metrics associated with increased mechanical strength and resistance to infection. Porcine acellular lung matrix is a novel tissue scaffold known to promote cell adherence while minimizing inflammatory reactions. In this study, we evaluate the capacity of porcine acellular lung matrix to sustain cellularization and neovascularization in a rat model of subcutaneous implantation and chronic hernia repair. We hypothesize that, compared to human acellular dermal matrix, porcine acellular lung matrix would promote greater cell infiltration and vessel formation. Following pneumonectomy, porcine lungs were processed and characterized histologically and by scanning electron microscopy to demonstrate efficacy of the decellularization. Using a rat model of subcutaneou implantation, porcine acellular lung matrices (n = 8) and human acellular dermal matrices (n = 8) were incubated in vivo for 6 weeks. To evaluate performance under mechanically stressed conditions, porcine acellular lung matrices (n = 7) and human acellular dermal matrices (n = 7) were implanted in a rat model of chronic ventral incisional hernia repair for 6 weeks. After 6 weeks, tissues were evaluated using hematoxylin and eosin and Masson's trichrome staining to quantify cell infiltration and vessel formation. Porcine acellular lung matrices were shown to be successfully decellularized. Following subcutaneous implantation, macroscopic vessel formation was evident. Porcine acellular lung matrices demonstrated sufficient incorporation and showed no evidence of mechanical failure after ventral hernia repair. Porcine acellular lung matrices demonstrated significantly greater cellular density and vessel formation when compared to human acellular dermal matrix. Vessel sizes were similar across all groups. Cell infiltration and vessel formation are well-characterized metrics of incorporation associated with improved surgical outcomes. Porcine acellular lung matrices are a novel class of acellular tissue scaffold. The increased cell and vessel density may promote long-term improved incorporation and mechanical properties. These findings may be due to the native lung scaffold architecture guiding cell migration and vessel formation. Porcine acellular lung matrices represent a new alternative for surgical wound healing applications where increased cell density and vessel formation are sought.

[1]Department of Surgery, Houston Methodist Hospital, Houston, TX, USA
[2]Surgical Advanced Technologies Lab, Department of Biomimetic and Regenerative Medicine, Houston Methodist Research Institute, Houston, TX, USA
[3]Department of Nanomedicine, Houston Methodist Research Institute, Houston, TX, USA
[4]Neurosensory Center, Department of Ophthalmology, Baylor College of Medicine, Houston, TX, USA
[5]Department of Internal Medicine, The University of Texas Medical Branch, Galveston, TX, USA

Corresponding author:
Joan E Nichols, Department of Internal Medicine, The University of Texas Medical Branch, 301 University Blvd, Marvin Graves Bldg, Rm 4.202, Galveston, TX 77555-0435, USA.
Email: jnichols@utmb.edu

Keywords
Porcine, hernia, alloderm neovascularization, musculoskeletal, incorporation

Received: 28 October 2015; accepted: 8 December 2015

Introduction

Metrics of bioprosthetic mesh incorporation are defined by cellular and vascular infiltration.[1] Increases in incorporation of these meshes have been shown to decrease infection and increase repair site strength.[2] Commercially available prosthetics include human acellular dermal matrix (ADM), porcine non-crosslinked and crosslinked ADM, and porcine urinary bladder matrix.[3,4] Despite the advances in techniques and technologies, recurrence rates following ventral hernia remain high.[5] This has prompted a search for both optimized materials and techniques for use in abdominal wall reconstruction.

One form of bioprosthetic mesh commonly used in abdominal wall reconstruction is human acellular dermal matrix (hADM).[6] While hADM and other ADMs were originally designed for indications other than abdominal wall reconstruction, they have been adopted by surgeons due to the need for prosthetics with better biologic and mechanical properties.[7] An ideal mesh avoids inflammation, is resistant to contamination, is non-toxic, is non-carcinogenic, and resists immune rejection.[8,9] Characteristics that are thought to contribute to the success of ADMs are their ability to cellularize and support robust neovascularization.[10,11] These features aid in their resistance to infection, a characteristic critical to their success. Natural scaffold materials hold great potential but have been hindered by poor long-term successes.[11–13] The shortcomings of these prosthetics are thought to be overcome by developing scaffolds that provide even more cellularization and vessel ingrowth.[13] Unfortunately, inherent lack of mechanical strength compared to synthetic materials or rapid loss of mechanical strength due to rapid remodeling may not be solved by enhancing incorporation.

While ADMs are the most popularly used bioprosthetics, other sources such as subintestinal submucosa, urinary bladder matrix, and bovine pericardium have been used in abdominal wall repair and have emerged as alternatives to ADMs.[14–16] Porcine acellular lung matrix (PALM) has been described as a natural scaffold capable of cell attachment and supporting maintenance of cell viability.[17,18] The lung as an organ has an extensive and well-defined vascular architecture.[19] PALMs are characterized by a predominance of collagen I and elastin capable of sustaining forces of mechanical ventilation for prolonged periods of time without change to the macro- or microstructure of the tissue.[17] Furthermore, PALMs were shown to have a minimal inflammatory response with minimal apoptosis of mesenchymal stem cells or human alveolar epithelial cells. Taken together, these features make PALMs a good candidate tissue scaffold for use in surgical wound healing applications.

In this study, we evaluate the capacity of PALMs to promote and sustain robust neovascularization and cellularization in vivo. To demonstrate this, we utilized an in vivo model of repair of chronic hernia and subcutaneous implantation to compare PALM to hADM with and without mechanical stresses. We hypothesized that PALM would have greater vessel formation and cell infiltration in in vivo models of rat subcutaneous implantation and chronic bridging ventral hernia repair.

Methods

Animals

To create the PALMs, two Yorkshire pigs weighing 52 kg were used for lung harvest and subsequent decellularization. For the implantation of PALMs and hADMs, a total of 18 rats were used. Four rats weighing approximately 300–315 g underwent subcutaneous implantation. Fourteen male Lewis rats weighing approximately 300–315 g underwent ventral hernia creation. After 30 days, animals were randomly assigned to receive repair with non-crosslinked hADM (Alloderm, "thick" (0.79- to 1.79-mm thick); LifeCell Corporation, Branchburg, NJ) or PALM. All rats were purchased from Charles River (Wilmington, MA), and all pigs were purchased from K Bar Livestock, LLC (Sabinal, TX) and housed at Houston Methodist Hospital Research Institute animal facility. The study was approved by the Institutional Animal Care and Use Committee at Houston Methodist Hospital Research Institute, and all investigators complied with National Research Council's *Guide for the Care and Use of Laboratory Animals.*

Lung harvest

Two Yorkshire pigs were used in the harvest of lungs. The animals underwent total pneumonectomy using the following procedure. A median sternotomy was made and the heart and lungs were exposed. The pulmonary artery (PA) was dissected free as was the left atrium of the heart. The animal was then humanely euthanized via exsanguination. To ensure all of the blood was removed from the vasculature of the lung, the PA was cannulated and normal saline 0.9% was infused until the effluent was clear. Once the effluent was clear of blood, the heart was dissected from the lung heart block. To allow for sufficient cannulation

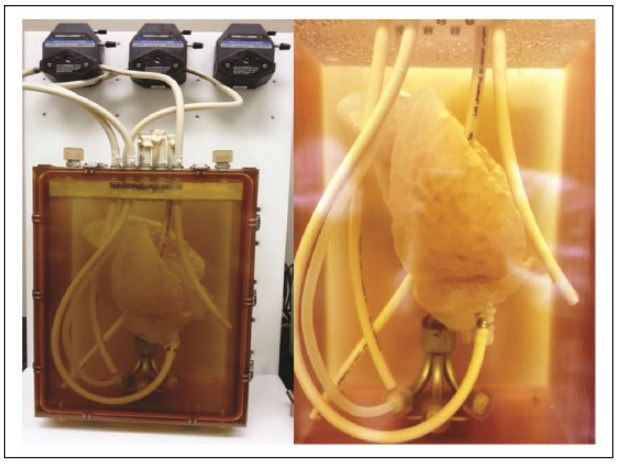

Figure 1. Decellularization bioreactor. Porcine lung in initial phases of decellularization within the decellularization chamber.

for decellularization, the PA was transected at its root. The lungs were then dissected from the chest wall using sharp and blunt dissection. The trachea was highly ligated and then the lungs were removed from the chest cavity and taken for decellularization.

Lung decellularization and characterization

After harvest, pig lungs were stored at −80°C for 1 month prior to decellularization. To allow for adequate thawing, lungs were placed in a refrigerator at 4°C for 3 days prior to being placed in the bioreactor chamber. Once lungs were thawed, the trachea and the PA were connected to separate cannulas and pumps (Figure 1). Lungs were decellularized using a modified version of the organ decellularization process that was previously explained by Nichols et al.[17] A perfusion decellularization process was employed using decreasing concentrations of sodium dodecyl sulfate (SDS) solution. Briefly, following canalization, SDS solution was perfused into the lungs at a rate of 100 mL/h for 3 days and then increased to 500 mL/h until day 7. To aid in the decontamination of the specimens, the lungs were perfused with a solution containing streptomycin (90 mg/mL), penicillin (50 U/mL), and amphotericin B (25 mg/mL) on day 7 prior to dissection.

To confirm the absence of cells in the lung matrix, four pieces of peripheral and parenchymal lung tissues were dissected, fixed in 10% buffered formalin, and paraffin embedded. Three non-consecutive 5-µm sections were mounted, sectioned, and stained by hematoxylin and eosin (H&E). Tissues were also evaluated using scanning electron microscopy (SEM) to confirm maintenance of the ultrastructure. To prepare the tissues for SEM, dissected lung parenchyma was fixed in 4% paraformaldehyde and dehydrated through a series of ethanol washes. Samples were then mounted and sputter coated for SEM.

Subcutaneous implantation

Rats were randomly allocated into treatment groups prior to surgery. Buprenorphine (0.03 mg/kg) and carprofen (5 mg/kg) were administered for preoperative analgesia. Anesthesia was induced and maintained using a 2.5%–3.0% isoflurane/oxygen mixture through a non-rebreather mask. Aseptic techniques were used for the duration of the surgery. In prone position, animals were shaved and the operative site prepped with a 2% chlorhexidine acetate solution. On the dorsal aspect of the animal (n = 4), four 1-cm incisions were made and the subcutaneous tissues were dissected to create a pouch. All tissues used underwent antibiotic perfusion at the end of decellularization and ultraviolet light sterilization prior to use. Each animal received two 2 cm × 2 cm pieces of PALM and two 2 cm × 2 cm pieces of hADM. The animals were recovered from anesthesia. Buprenorphine (0.03 mg/kg) and carprofen (5 mg/kg) were administered for postoperative analgesia. Postoperative daily physical examinations assessing for signs of bleeding and infection as well as daily weight measurements were performed for the first week. Physical examination involved visual inspection and palpation of the dorsum for seroma formation and infection. Animals that lost more than 10% weight were treated with saline injections and moist pellets. Rats were euthanized at 6 weeks using inhalant carbon dioxide at 70%. At which time, the rats were euthanized for tissue harvest.

Chronic hernia creation and repair

Rats were randomly allocated into treatment groups prior to surgery. Then, abdominal wall defect creation was performed as previously described.[20] Buprenorphine (0.03 mg/kg) and carprofen (5 mg/kg) were administered for preoperative analgesia. Anesthesia was induced and maintained using a 2.5%–3.0% isoflurane/oxygen mixture through a non-rebreather mask. Aseptic techniques were used for the duration of the surgery. To create the abdominal wall defect, all rats had a 3-cm midline skin incision and a 3-cm skin flap raised using sharp dissection. A full-thickness abdominal midline fascia/muscle/peritoneum defect measuring 2 cm in length was then completed. The skin was approximated and stapled leaving the defect unrepaired. Fascial defects were allowed to mature over 30 days. The animals were monitored by physical examination and weighed daily for the first 10 days following the procedure and then once weekly. Exclusion collars were applied for 5 days to ensure the animals did not disrupt the incision in the early postoperative period. After 14 days, the staples were removed.

Abdominal wall defect repair

Thirty days after the abdominal wall defect creation surgery, hernia repair with either PALM or hADM was

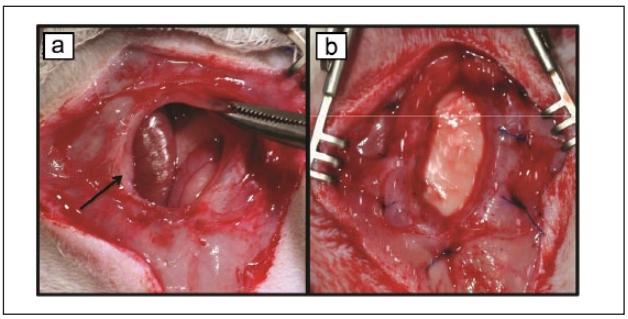

Figure 2. Chronic hernia repair. (a) Following dissection of intra-abdominal contents, scarred borders of chronic hernia are visible (arrow). (b) Hernia following underlay repair with PALM.

performed. Protruding viscera was freed from the fascial edges and the borders defined. A 3 cm × 2 cm piece of PALM or hADM was customized to the shape of the fascial defect in order to allow for 5 mm of overlap between the muscle and the mesh. Then, an underlay repair was performed, in which the mesh was placed between the contents of the abdominal cavity and the abdominal wall. The mesh was fixed to the fascia with the use of eight transfascial 5-0 Prolene sutures spaced equally apart (Figure 2). The skin was then closed using skin staples. Exclusion collars were then reapplied and the animals returned to their cages. Buprenorphine (0.03 mg/kg) and carprofen (5 mg/kg) were administered for postoperative analgesia. Postoperative daily physical examinations assessing for signs of bleeding and infection as well as daily weight measurements were performed for the first week. Physical examination involved visual inspection and palpation of the abdominal wall for seroma formation and herniation of abdominal viscera. Animals that lost more than 10% weight were treated with saline injections and moist pellets.

Euthanization and specimen harvest

Six weeks postoperation, the animals were euthanized using 70% inhaled carbon dioxide and confirmed with thoracotomy. Tissue samples were harvested with an equal amount of adjacent native abdominal wall tissue. The specimens were then fixed in 10% buffered formalin to evaluate gross histology. Fixed tissues were then trimmed of excess tissue and embedded in paraffin.

Histopathology

All paraffin-embedded tissues from in vivo implantation were serially sectioned into 5-μm sections. To assess neovessel formation and tissue deposition, three non-consecutive sections were routinely stained with H&E (Sigma-Aldrich, St. Louis, MO) and Masson's trichrome. After staining, the tissue sections were assessed. To quantify neovessel formation at 6 weeks, 9 fields of view (1 mm × 1 mm) per Masson's trichrome stained and vascular structures were blindly quantified. Cell infiltration of the scaffolds was assessed by quantifying the number of cells per each field of view (0.5 mm × 0.5 mm) and 9 fields of view were chosen in corresponding areas to those evaluated for neovascularization. To assess vessel size, the seven largest vessels per field of view were measured for diameter and recorded.

Statistics

All data are presented as mean ± standard deviation. Statistical analysis was carried out using GraphPad Prism version 5.0 (GraphPad Software, San Diego, CA). A p value less than 0.05 was considered statistically significant. Significance in cellular infiltration, vessel infiltration, and vessel diameter was determined using one-way analysis of variance and Tukey's test for post hoc evaluation when significance was found.

Results

Characterization of decellularization

Decellularization of the pig lungs was evaluated using H&E staining which showed loss of cells throughout the tissue. SEM also confirmed the absence of cells (Figure 3(b)). No visible cellular tissue remained in all central and peripheral parenchymal tissues. SEM analysis showed the highly organized structure of the lung that contributes to its high potential for neovascularization (Figure 3(c)). The architecture of the lung is retained following decellularization with only minimal collapse of bronchial structures (Figure 3(d)).

Gross histology

Macroscopic vessel formation was clearly visible on both PALM and hADM after 6 weeks in vivo (Figure 4). Additionally, neither matrix had significant resorption. When examining the ventral hernia repair, it was evident that both tissue matrices were present at the end of the study (Figure 5). However, the hADM implants did appear to bulge more than the PALM implants. This qualitative finding correlates with other findings for increased incorporation of the PALM compared to hADM. Additionally, no PALMs experienced mechanical failure or rupture for up to 6 weeks in vivo, and all PALMs appeared to be intact at necropsy.

Cellular infiltration

Bioprosthetic cellular infiltration is a critical metric of incorporation.[1] Following subcutaneous implantation, PALMs demonstrated a significantly greater number of

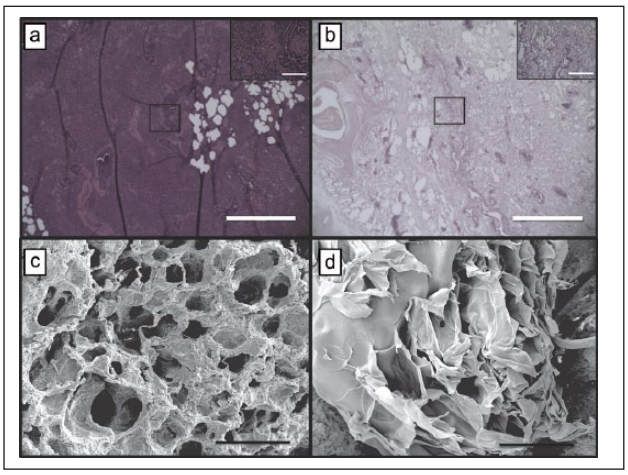

Figure 3. Characterization of decellularization. Hematoxylin and eosin staining at (a) day 0 and (b) day 7 confirm complete decellularization following SDS baths (scale bar, 150 µm; inset 40× magnification; scale bar, 20 µm). (c) Well-formed and cellularized tubular vascular structures are in lung tissue prior to processing (scale bar, 100 µm). (d) Decellularized vascular structures retain tubular morphology and architecture (scale bar, 100 µm).

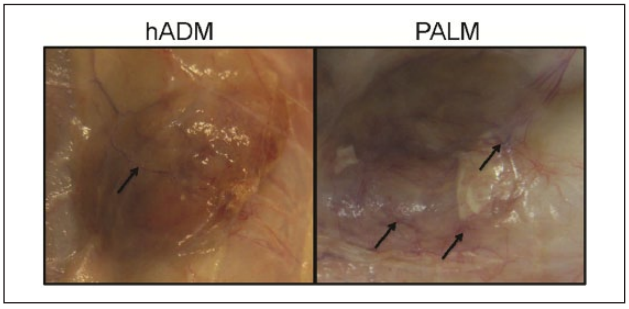

Figure 4. Subcutaneous implantation. Macroscopic vessel infiltration (arrows) is seen following 6 weeks of subcutaneous implantation.

cells compared to hADM at 6 weeks (Figure 6). PALMs had a homogeneous concentration of 1585 ± 163 cells per 500 µm^2, while hADM had a significantly lower concentration of cells with 400 ± 183 cells per 500 µm^2 ($p < 0.001$). Furthermore, the distribution of cells in the hADM was more concentrated on the periphery, while PALM had a more homogeneous distribution. These findings translated to significantly greater cells infiltrated in PALMs implanted for chronic ventral hernia repair. Following 6 weeks of implantation, PALM cellularization was 1663 ± 228 cells per 500 µm^2 compared to 350 ± 230 cells per 500 µm^2 seen in hADM ($p < 0.001$; Figure 7).

Vessel formation

Vessel ingrowth is known to be a strong predictor of incorporation, subsequent resistance to infection, and increased

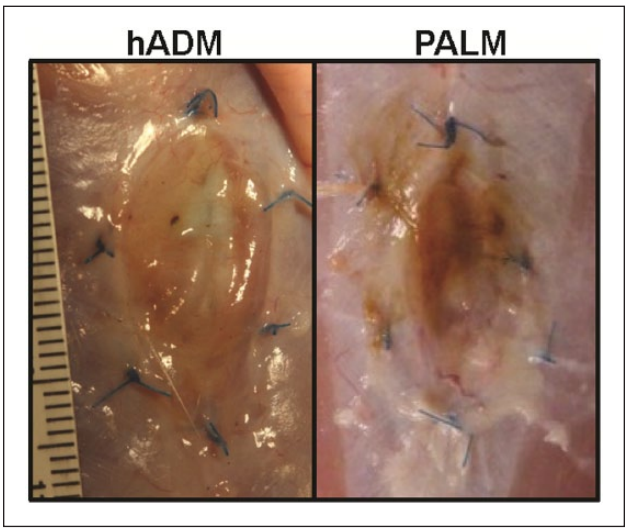

Figure 5. PALM and hADM in hernia repair. Following 6 weeks of incubation under the mechanical stresses of abdominal wall implantation, both hADM and PALM did not rupture or breakdown. Bulge was evident in the hADM group. Both acellular matrices demonstrated incorporation.

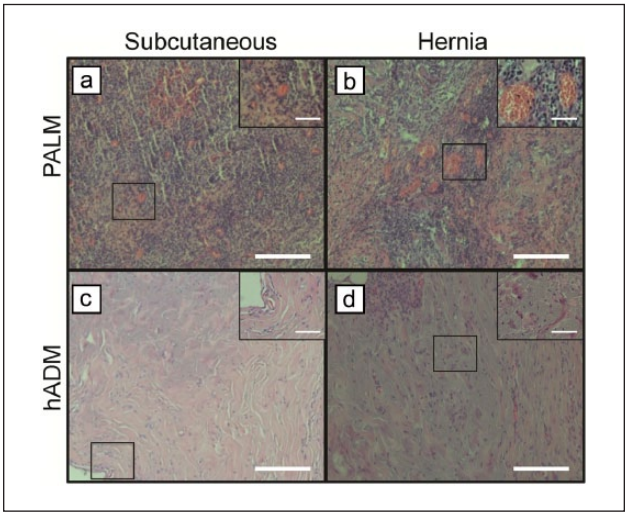

Figure 6. PALMs demonstrate increased cell infiltration. Representative images of H&E-stained implants following (a, c) subcutaneous implantation and (b, d) implanted for hernia repair. PALMs demonstrate a greater cellularity compared to hADM (scale bar, 50 µm) (inset 40× magnification; scale bar, 20 µm).

mechanical strength.[2,10] Subcutaneous implantation of PALM showed a significantly greater number of vessels per field of view (Figure 8). PALM mesh had 57 ± 13 vessels per 1 mm^2. This was approximately six times the amount of vessels per field of view compared with hADM, which demonstrated only 9 ± 5 vessels per 1 mm^2. Vessel ingrowth seen in hernia repair was similar to that seen in subcutaneous implantation. PALMs showed a significantly larger amount of vessels per 1 mm^2 (46 ± 10) compared to

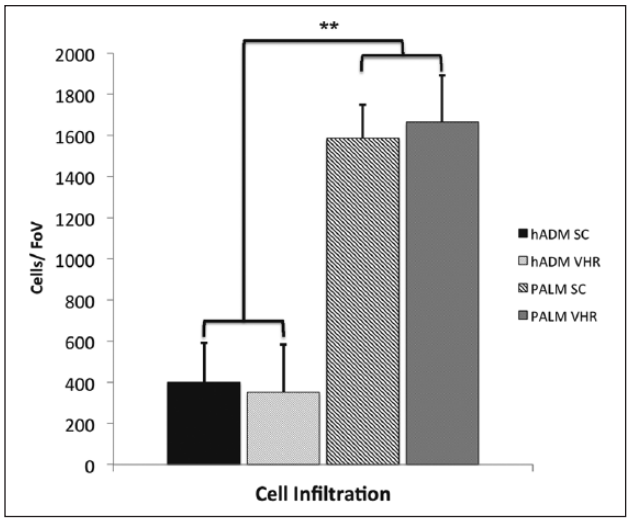

Figure 7. Mean cell density (±standard deviation) in PALMs and hADM implanted for 6 weeks in rat model of chronic hernia repair (FoV = 0.5 mm²; **p < 0.001).

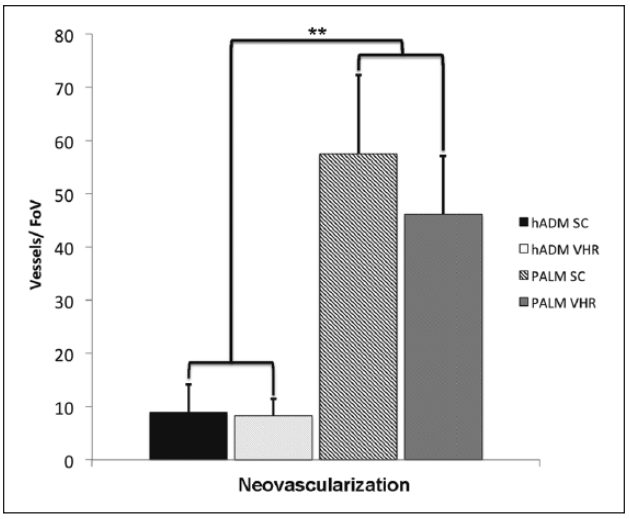

Figure 9. Mean vessel density (±standard deviation) in PALMs and hADM implanted for 6 weeks in rat model of chronic hernia repair (FoV = 1 mm²; **p < 0.001).

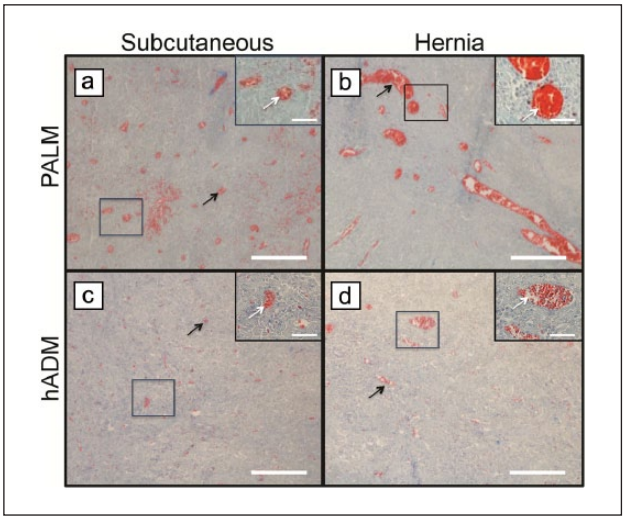

Figure 8. PALMs demonstrate greater vessel formation. Representative images of Masson's trichrome-stained implants following (a, c) subcutaneous implantation and (b, d) implanted for hernia repair. PALMs had greater vessel infiltration (white and black arrows) compared to hADM (scale bar, 50 μm) (inset 40× magnification; scale bar, 20 μm).

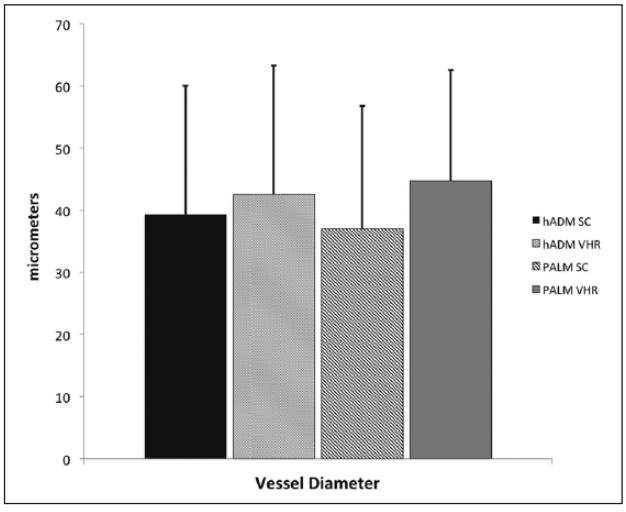

Figure 10. Mean vessel diameter in PALMs and hADM demonstrates similar size following 6-week implantation in chronic hernia.

hADM (8 ± 3; p < 0.001; Figure 9). Vessel diameter of the seven largest vessels per field of view was also quantified to assess whether vessel diameter was affected. No difference in vessel diameter was seen between groups in the subcutaneous implantation and hernia repair (Figure 10).

Discussion

Over 4 million laparotomies are performed annually in the United States, with 2%–30% of these resulting in incisional hernia.[21] From these, approximately 360,00 hernias require repair.[22] The most commonly used prosthetics continue to be synthetic material–based devices.[23] These are plagued with a multitude of complications ranging from contraction to erosion and evisceration.[24] To address this, surgeons have looked to bioprosthetics as a solution to overcome the disadvantages of synthetic prosthetics. While biologically derived or biological material–based non-synthetic devices have shown some success, their place in the operative theater has been limited to repair in which infection is present.[25] Otherwise, their efficacy has not been demonstrated for repair of bridging hernias. This is thought to be due, in part, to the limited incorporation of the mesh itself.

hADM has been extensively studied within the context of abdominal wall reconstruction.[25] However, its efficacy in bridging hernia repair has failed to be realized due to its resorption and accelerated loss of mechanical strength, leading to bulge and hernia recurrence.[26] Porcine dermis–based prosthetics, such as non-crosslinked and crosslinked ADMs, have become not only increasingly popular but also ultimately fail to achieve a durable long-term repair in bridging hernia reconstruction. The capacity of bioprosthetics to resist infection and undergo cellular infiltration and neovascularization is a significant advantage of this class of prosthetics. However, while there is limited high-level data regarding mechanism of action or long-term efficacy, long-term implantation of hADM has been shown to result in bulge and repair laxity.[27,28]

PALM is a novel matrix originally conceived for use in pulmonary regeneration.[17] Metrics for effective incorporation have been described and validated.[1] Because of the native vascular architecture, we sought to understand its capacity for cellularization and neovascularization, important metrics of incorporation, in a subcutaneous implantation and ventral hernia repair rat model. This would allow for an understanding of the ability of PALM to cellularize and neovascularize in both a non-mechanical and mechanically stressed system. PALMs demonstrated a greater potential for cellularization and neovessel formation, characteristics that would predispose it to greater incorporation and thus long-term mechanical stability. These findings suggest that the vascular network architecture inherent to the lung anatomy allows for more cellular infiltration and vessel formation. The similar sizes in vessels indicate that the normal biological process of vascularization was accelerated in the PALMs. These findings carry great significance for both wound healing applications and abdominal wall repair where the need for vessel ingrowth would enhance healing and resistance to infection.

We observed that by 6 weeks, PALM implants did not undergo significant bulge or mechanical failure. This finding is critical as bulge by this time point is an indicator of long-term mechanical failure.[21] Bulge is a result of the delicate interplay of collagen degradation and deposition.[29,30] Cell and vessel invasion is thought to play a critical role in this. This study highlights that the native architecture of the bioprosthetic can significantly affect these important biological outcomes. The lung, compared to the dermis, has significantly greater vascularity. As the lung's main function is inherently for exchange of oxygen and carbon dioxide from the blood, there is a vast interconnected network of vessels that following decellularization are retained for infiltration. We believe this to be the major feature predisposing PALMs to enhanced incorporation.

One limitation to this study is the lack of mechanical strength evaluation. One could suppose that with increased incorporation, greater mechanical strength would be achieved. This would translate to decreased rates of recurrence. This is the current subject of investigation. Another shortcoming of the study is the short duration. To properly assess the efficacy of a repair to withstand the mechanically stressed cycling of the abdominal wall, a longer time point must be achieved. While this was out of the scope of this pilot study, it is also a focus for subsequent validation studies for PALMs. Follow-up studies with greater numbers are currently underway.

In summary, this pilot study demonstrates the feasibility of PALMs for use in wound healing and abdominal wall repair. Our findings suggest that PALMs can potentially be an effective wound healing agent because of their ability to robustly cellularize and promote vessel ingrowth. When compared to extensively studied commercially available bioprosthetics such as hADM, we find that PALMs are superior in their ability to promote incorporation. While more studies are needed to understand their long-term efficacy and mechanical strength, this pilot study validates their potential as a novel wound healing scaffold.

Conclusion

Surgical wounds continue to be plagued by a lack of suitable healing aids that promote cellularization and neovascularization. PALM, through the inherent and extensive vascular architecture, is an excellent candidate to enhance the biological processes of wound healing. This study demonstrates the efficacy of PALM to promote metrics associated with enhanced incorporation. PALM was superior to hADM in promoting angiogenesis and cell infiltration. These findings collectively suggest that studies involving more animals and comprehensive mechanical and molecular analyses are merited.

Acknowledgements

The authors thank the scanning electron microscopy core for their commitment of superior imaging and assistance in acquisition of high-quality images. They also thank the histology core for providing excellent services in the processing and staining of tissues.

Declaration of conflicting interest

The author(s) declared no potential conflicts of interest with respect to the research, authorship, and/or publication of this article.

Funding

Dr Joseph Fernandez-Moure is currently funded by a grant from DSM biomedical.

References

1. Campbell KT, Burns NK, Ensor J, et al. Metrics of cellular and vascular infiltration of human acellular dermal matrix in ventral hernia repairs. *Plast Reconstr Surg* 2012; 129: 888–896.

2. Milburn ML, Holton LH, III, Chung TL, et al. Acellular dermal matrix compared with synthetic implant material for repair of ventral hernia in the setting of peri-operative *Staphylococcus aureus* implant contamination: a rabbit model. *Surg Infect* 2008; 9: 433–442.
3. Baumann DP and Butler CE. Bioprosthetic mesh in abdominal wall reconstruction. *Semin Plast Surg* 2012; 26: 18–24.
4. Bolland F, Korossis S, Wilshaw SP, et al. Development and characterisation of a full-thickness acellular porcine bladder matrix for tissue engineering. *Biomaterials* 2007; 28: 1061–1070.
5. Flum DR, Horvath K and Koepsell T. Have outcomes of incisional hernia repair improved with time? A population-based analysis. *Ann Surg* 2003; 237: 129–135.
6. Campbell KT, Burns NK, Rios CN, et al. Human versus non-cross-linked porcine acellular dermal matrix used for ventral hernia repair: comparison of in vivo fibrovascular remodeling and mechanical repair strength. *Plast Reconstr Surg* 2011; 127: 2321–2332.
7. Sheridan RL and Choucair RJ. Acellular allogenic dermis does not hinder initial engraftment in burn wound resurfacing and reconstruction. *J Burn Care Rehabil* 1997; 18: 496–499.
8. Hamer-Hodges D and Scott N. Surgeon's workshop. Replacement of an abdominal wall defect using expanded PTFE sheet (Gore-tex). *J R Coll Surg Edinb* 1985; 30: 65–67.
9. Cevasco M and Itani KM. Ventral hernia repair with synthetic, composite, and biologic mesh: characteristics, indications, and infection profile. *Surg Infect* 2012; 13: 209–215.
10. Wu X, Kathuria N, Patrick CW, et al. Quantitative analysis of the microvasculature growing in the fibrin interface between a skin graft and the recipient site. *Microvasc Res* 2008; 75: 119–129.
11. Eppley BL. Experimental assessment of the revascularization of acellular human dermis for soft-tissue augmentation. *Plast Reconstr Surg* 2001; 107: 757–762.
12. Campbell K, Burns N, Rios C, et al. 167A: In vivo comparison of human acellular dermal matrix and non-cross-linked porcine acellular dermal matrix. *Plast Reconstr Surg* 2010; 125: 111.
13. Campbell KT, Burns NK and Butler CE. Evaluation of human acellular dermal matrices for the metrics of cellular and vascular infiltration. *Plast Reconstr Surg* 2010; 126: 85–86.
14. Mofid MM, Meininger MS and Lacey MS. Veritas® bovine pericardium for immediate breast reconstruction: a xenograft alternative to acellular dermal matrix products. *Eur J Plast Surg* 2012; 35: 717–722.
15. Valerio IL, Campbell P, Sabino J, et al. The use of urinary bladder matrix in the treatment of trauma and combat casualty wound care. *Regen Med* 2015; 10: 611–622.
16. Ansaloni L, Catena F, Gagliardi S, et al. Hernia repair with porcine small-intestinal submucosa. *Hernia* 2007; 11: 321–326.
17. Nichols JE, Niles J, Riddle M, et al. Production and assessment of decellularized pig and human lung scaffolds. *Tissue Eng Part A* 2013; 19: 2045–2062.
18. Nichols JE, Niles JA and Cortiella J. Production and utilization of acellular lung scaffolds in tissue engineering. *J Cell Biochem* 2012; 113: 2185–2192.
19. DeMello DE, Sawyer D, Galvin N, et al. Early fetal development of lung vasculature. *Am J Respir Cell Mol Biol* 1997; 16: 568–581.
20. Fernandez-Moure JS, Van Eps JL, Menn ZK, et al. Platelet rich plasma enhances tissue incorporation of biologic mesh. *J Surg Res* 2015; 199: 412–419.
21. Schoenmaeckers EJ, Wassenaar EB, Raymakers JT, et al. Bulging of the mesh after laparoscopic repair of ventral and incisional hernias. *JSLS* 2010; 14: 541–546.
22. Read RC and Yoder G. Recent trends in the management of incisional herniation. *Arch Surg* 1989; 124: 485–488.
23. Brown C and Finch J. Which mesh for hernia repair? *Ann R Coll Surg Engl* 2010; 92: 272–278.
24. Harrell AG, Novitsky YW, Peindl RD, et al. Prospective evaluation of adhesion formation and shrinkage of intra-abdominal prosthetics in a rabbit model. *Am Surg* 2006; 72: 808–814.
25. Holton LH, III, Kim D, Silverman RP, et al. Human acellular dermal matrix for repair of abdominal wall defects: review of clinical experience and experimental data. *J Long Term Eff Med Implants* 2005; 15: 547–558.
26. Sandor M, Xu H, Connor J, et al. Host response to implanted porcine-derived biologic materials in a primate model of abdominal wall repair. *Tissue Eng Part A* 2008; 14: 2021–2031.
27. Bluebond-Langner R, Keifa ES, Mithani S, et al. Recurrent abdominal laxity following interpositional human acellular dermal matrix. *Ann Plast Surg* 2008; 60: 76–80.
28. Lee EI, Chike-Obi CJ, Gonzalez P, et al. Abdominal wall repair using human acellular dermal matrix: a follow-up study. *Am J Surg* 2009; 198: 650–657.
29. Brown BN, Londono R, Tottey S, et al. Macrophage phenotype as a predictor of constructive remodeling following the implantation of biologically derived surgical mesh materials. *Acta Biomater* 2012; 8: 978–987.
30. Connor J, McQuillan D, Sandor M, et al. Retention of structural and biochemical integrity in a biological mesh supports tissue remodeling in a primate abdominal wall model. *Regen Med* 2009; 4: 185–195.